Re-analysis of the Cassini RPWS/LP data in Titan's ionosphere. Part II: statistics on 57 flybys

Audrey Chatain, J.-E. Wahlund, O. Shebanits, L. Z. Hadid, M. Morooka, N. J. T. Edberg, O. Guaitella, Nathalie Carrasco

Re-analysis of the Cassini RPWS/LP data in Titan's ionosphere. Part II: statistics on 57 flybys.

A. Chatain[1,2], J.-E. Wahlund[3], O. Shebanits[3,4], L. Z. Hadid[2,3], M. Morooka[3], N. J. T. Edberg[3], O. Guaitella[2], and N. Carrasco[1]

[1] Université Paris-Saclay, UVSQ, CNRS, LATMOS, Guyancourt, France.

[2] LPP, Ecole polytechnique, Sorbonne Université, Institut Polytechnique de Paris, CNRS, Palaiseau, France.

[3] Swedish Institute of Space Physics, Uppsala, Sweden.

[4] Imperial College London, United-Kingdom.

Corresponding author: Audrey Chatain (audrey.chatain@ens-paris-saclay.fr)

Key Points:

- Three main cold electron populations are detected by the Cassini Langmuir probe in Titan's ionosphere below 1200 km altitude.
- One population is attributed to background thermal electrons and one to electrons linked to the photo-induced ion chemistry.
- A third electron population, observed on dayside below 1200 km, could be photo- or thermo-emitted from dust grains.

Abstract

The ionosphere of Titan hosts a complex ion chemistry leading to the formation of organic dust below 1200 km. Current models cannot explain the observed electron temperature in this dusty environment. To get new clues, we re-analyzed the data taken in the ionosphere of Titan by the Cassini Langmuir probe (LP), part of the Radio and Plasma Wave Science (RPWS) package. A first paper (Chatain et al., n.d.) introduces the new analysis method and discusses the detection of 4 different electron populations. In this second paper, we present a statistical study of the whole LP dataset below 1200 km and gives clues on the origin of the 4 populations. One small population is attributed to photo- or secondary electrons emitted from the surface of the probe boom. A second population is systematically observed, at a globally constant density (~500 cm^{-3}), and is attributed to background thermalized electrons. The two last populations increase in density with pressure, solar illumination and extreme UV flux. The third population is observed with varying densities at all altitudes (at least up to 1400 km) and solar zenith angles except on the far nightside (SZA > ~140°), with a maximum density of 2700 cm^{-3}. It is therefore certainly related to photo-ionization and its subsequent active ion chemistry. Finally, a fourth population detected only on the dayside and below 1200 km reaching up to 2000 cm^{-3} could be photo- or thermo-emitted from dust grains.

1 Introduction

Titan's ionosphere is a complex environment, partly governed by an active ion chemistry leading to the formation of organic dust grains (Vuitton et al., 2019; Waite et al., 2007). From 2004 to 2017, the ionospheric plasma has been investigated *in situ* by many instruments on-board the Cassini mission, such as the ion and neutral mass spectrometer INMS (Cui et al., 2009; Magee et al., 2009; Mandt et al., 2012; Waite et al., 2005, 2007), the Cassini plasma spectrometer CAPS (Coates et al., 2007, 2009; Crary et al., 2009; Wellbrock et al., 2013, 2019) and the radio and plasma wave science (RPWS) package.

In particular, RPWS was designed to continue and improve the first radio and plasma wave measurements in the Saturn system, done by Voyager 1 and 2 (Gurnett et al., 1981; Scarf et al., 1982). This instrument aimed to study radio emissions, plasma waves, thermal plasma and dust (Gurnett et al., 2004). It was formed by a suite of antennas and sensors, among which a Langmuir probe, built by the Swedish Institute of Space Physics (IRF). The Langmuir probe measures low energy charged particles in ionized environments, and took *in situ* measurements in the magnetosphere and ionosphere of Titan at the occasion of 126 flybys. Electron density and temperature were deduced from these measurements (Ågren et al., 2009; Edberg et al., 2010, 2013, 2015; Wahlund et al., 2005). However, electron temperature measurements are not well reproduced by models of the ionosphere of Titan below 1200 km: model results give electrons too cold by a factor of 2-3 (Galand et al., 2014; Mukundan & Bhardwaj, 2018; Richard et al., 2011; Shebanits et al., 2017a; Vigren et al., 2013, 2016).

In the goal to get additional clues from the electron density and temperature measurements, we re-analyzed Langmuir probe dataset in the ionosphere, during the 13 years of the mission. This work is presented in two parts. In a first paper (Chatain et al., n.d.), further referred as 'paper I', we detailed the method used for the re-analysis of the data, and in a second paper (this one), we present the results obtained for the complete Cassini dataset. Paper I showed that several electron populations are systematically measured by the Langmuir probe in the ionosphere of Titan. Depending on the solar illumination and the altitude probed, 2 to 4 populations with different densities, temperatures and potentials were detected.

The detection of several electron populations is not unusual. Previous works observed 2 to 3 electron populations in the upper atmosphere of Venus (Intriligator et al., 1979), in Mars ionosphere (Hanson & Mantas, 1988; Mitchell et al., 2000), in the ionized environment of the comet 67P/Churyumov-Gerasimenko (Eriksson et al., 2017), in Saturn's magnetosphere (Schippers et al., 2008) and at Enceladus (Tokar et al., 2006). In all these cases, a cold electron population, thermalized through collisions, cohabits with hot suprathermal electrons coming from the solar wind, the magnetosphere of Saturn or photo-ionization. The main difference in the case of the ionosphere of Titan is that all the four electron populations observed are cold (<1 eV). Indeed, in these conditions models predict that all electrons should be thermalized (Galand et al., 2014). Previous works studying Langmuir probe data in Titan's ionosphere (Ågren et al., 2009; Edberg et al., 2010, 2013, 2015; Wahlund et al., 2005) already used 2 and sometimes 3 electron populations to fit the data, without investigating on their variations and origins.

To closely investigate the origins of the 4 populations detected, we analyzed the whole Langmuir probe dataset in the ionosphere of Titan and searched for correlations with the EUV flux (computed by Shebanits et al., 2017b) and the positive and negative ion densities (deduced from a multi-instrument study by Shebanits et al., 2016). Section 2 presents the Langmuir probe dataset, section 3 shows the electron density and temperature results, section 4 studies correlations and sections 5 discusses the origin of the four populations based on the results of the previous sections.

2 Materials and Methods

2.1 Langmuir probe data in Titan's ionosphere

The Langmuir probe (LP) was part of the Radio and Plasma Wave Science (RPWS) package on-board Cassini (Gurnett et al., 2004). In this study we used data from the voltage sweep mode, one of the three operational modes of the probe. In this mode, the voltage is swept between +4 and -4 V and the current collected by the probe is measured. Further details are given in paper I.

In this work, we focused on the region below 1200 km in altitude. We analyzed the 57 Cassini flybys that went below this altitude (T5, 16-21, 23, 25-30, 32, 36, 39-43, 46-51, 55-59, 61, 65, 70-71, 83-88, 91-92, 95, 100, 104, 106-108, 113, 117-121, 126). During these flybys, Cassini spent ~15 min below 1400 km, during which it continuously acquired voltage sweeps (26-30 in total, at different altitudes). The spatial resolution is limited to ~3 km due to the spacecraft motion at ~6 km/s. The flybys happened at various seasons, solar zenith angles (SZA) and latitudes. Their characteristics are represented in Figure 1. More precisely, the Cassini mission lasted 13 years and observed two seasons: it arrived in the system of Saturn in 2004 just after the northern hemisphere winter and stayed until the summer solstice in 2017. The vernal equinox marqued the middle of the total mission in 2010.

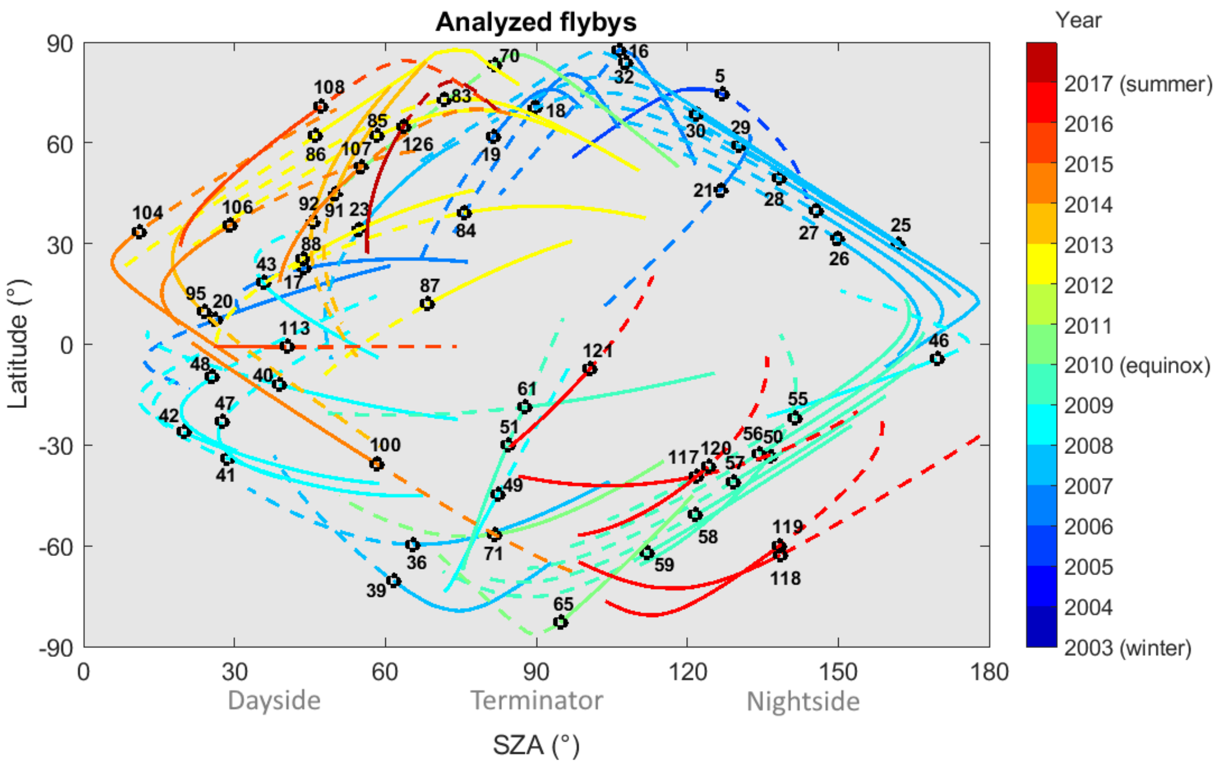

Figure 1. Trajectories of the 57 flybys analyzed as a function of solar zenith angle, latitude and year. Closest approach is marked by black circles.

2.2 Method to deduce electron density and temperature from voltage sweeps

The electron characteristics in the ionosphere are derived from the voltage sweep analysis. The acquired current is corrected for the positive ion current to obtain the electron current. Then, the electron current is fitted assuming that the electron populations have a Maxwellian speed distribution and using the Orbital Motion Limited (OML) theory and a Sheath Limited (SL) correction. The method is discussed in details in paper I. Depending on the altitude and the solar illumination, 2 to 4 electron populations are detected, and their densities and temperatures are retrieved with generally 10% to 30% uncertainties (confidence interval at 95%). The lower detection limit of the probe in temperature is 0.015 eV (~175 K), due to the electrical work function for the probe coating material (TiN, ~15 mV rms) (Veszelei, 1997). The four detected populations are named P_1, P_2, P_3 and P_4 according to their increasing potentials from P_1 to P_4 (see paper I).

3 Results: electron densities and temperatures

3.1 Statistics on 57 flybys

Figure 2 gives the results on electron density and temperature obtain for each of the 4 populations for the 57 flybys studied. Each of the four populations have a different behavior with altitude, which are described below.

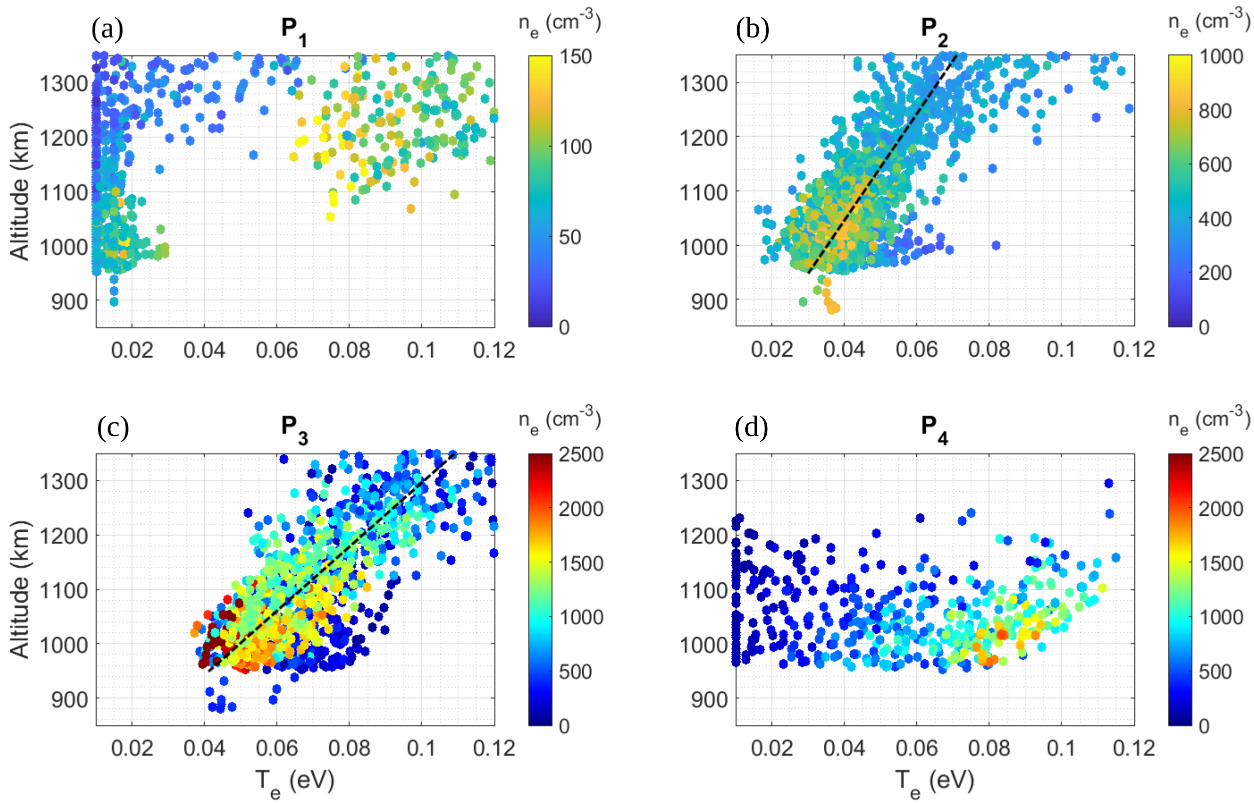

Figure 2. Electron temperature and density as function of altitude for the four electron populations: (a) P_1, (b) P_2, (c) P_3 and (d) P_4. Data from 57 flybys. Linear altitude trends are indicated with a black dashed line in the cases of P_2 and P_3 (respectively at -0.010 eV/100 km and -0.017 eV/100 km).

P_1 (Figure 2a) is a population with a very low density (< 150 cm^{-3}). Two different behaviors are observed: the low temperature electrons (< 0.02 eV, 230 K) at all altitudes, and hotter electrons (0.07 – 0.12 eV; 810-1390 K) found only above 1100 km.

P_2 electrons (Figure 2b) reach temperatures mainly between 0.025 and 0.08 eV (290-930 K), with a maximum at 0.12 eV (1390 K). P_3 electrons (Figure 2c) are generally hotter, with a minimum at 0.04 eV (460 K). P_2 and P_3 show in average a linear decrease in temperature with a decreasing altitude. The altitude trends for the two populations are different: estimations give -0.010 eV (115 K) / 100 km for P_2 and -0.017 eV (200 K) / 100 km for P_3. Therefore, the electrons of P_3 are hotter, but their temperature decreases with altitude ~70% faster than the electrons of P_2. Higher densities are globally found at lower altitudes.

P_4 electrons (Figure 2d) have the particularity to appear only below ~1250-1200 km altitude, with a large range of temperatures, between 0.01 and 0.12 eV (120-1390 K). Higher densities are correlated with higher temperatures.

3.2 Variations of the electron density with SZA and altitude

3.2.1 Trends for the four populations

The electron populations have a strong dependence on Solar Zenith Angle (SZA). Figure 3 shows the results in terms of electron density.

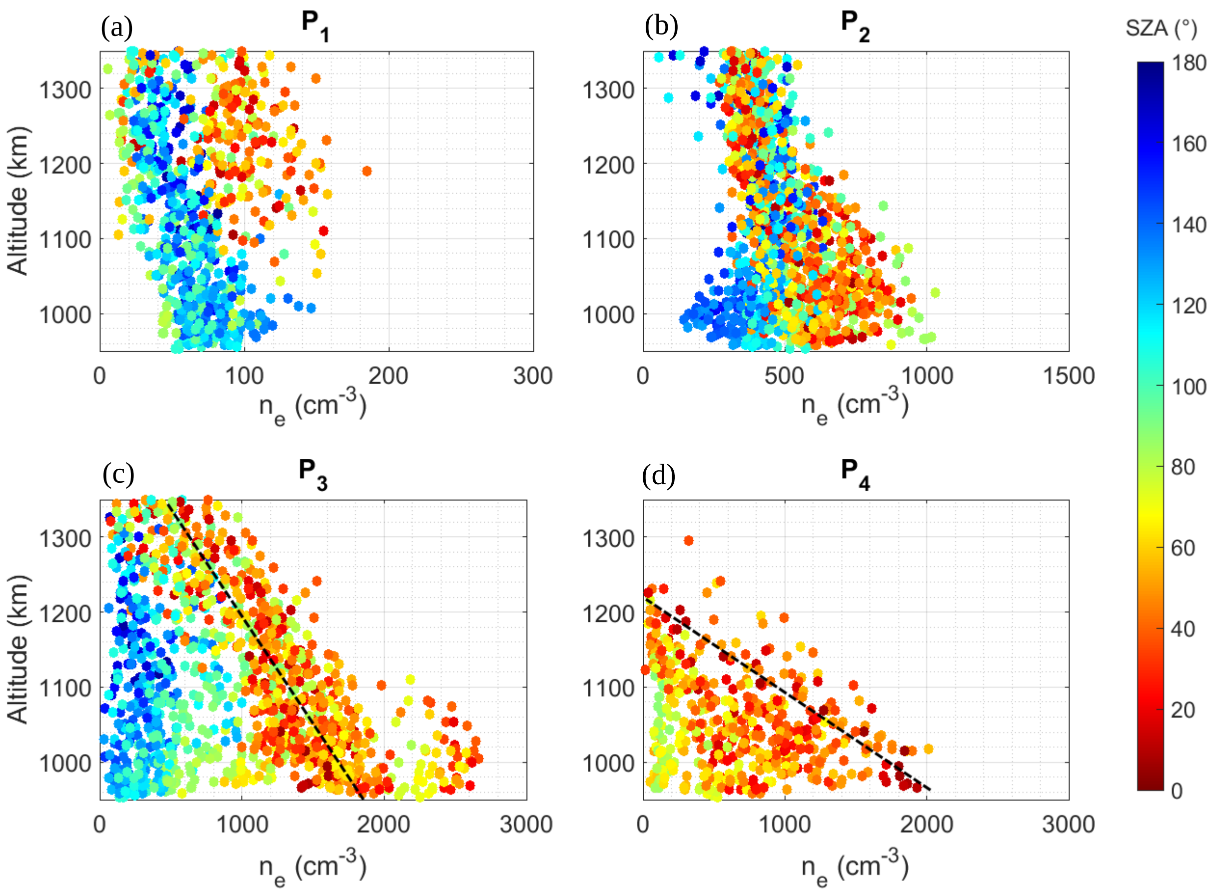

Figure 3. Electron density as a function of altitude and Solar Zenith Angle (SZA) for the four electron populations: (a) P_1, (b) P_2, (c) P_3 and (d) P_4. Data from 57 flybys. Linear altitude trends are indicated with a black dashed line in the cases of P_3 and P_4 (respectively at +350 cm^{-3}/100 km and +770 cm^{-3}/100 km).

P_1 electrons (Figure 3a) at low SZA are only observed at high altitudes. Their density remains low (~100 cm^{-3}) in any condition. P_2 electron density (Figure 3b) stays globally constant around 500 cm^{-3} at all altitudes and all SZA. Only a small shift is observed at low altitude, with higher densities on the dayside (~700 cm^{-3}) and lower densities on the nightside (~400 cm^{-3}). The effect of SZA is stronger on P_3 and P_4. While the density of P_3 (Figure 3c) is globally constant with altitude on the nightside (~300 cm^{-3}), it strongly increases with decreasing altitude on the day side, with a slope of +350 cm^{-3} / -100 km (up to ~1900 cm^{-3} at 950 km). For P_4 (Figure 3d), the maximum density reached at each altitude increases strongly with decreasing altitude and SZA. In the case of SZA < 20°, the increase of density is about +770 cm^{-3} / -100 km. The increase of the total electron density at low solar zenith angle was already observed by Ågren et al. (2009) on flybys from T16 to T42. The re-analysis of the complete dataset confirmed their observation and showed that the total density increase is due to the increase of P_3 electrons and the apparition of P_4 electrons.

3.2.2 Repartition of the negative charge carriers

The four electron populations have densities varying with altitude and SZA. Figure 4 synthesizes the average repartition of negative charge carrier densities (electrons and negative ions) with altitude and SZA. Negative ion values are from Shebanits et al. (2016). Above 1050 km in altitude, the negative charges essentially come from the electrons. On the opposite, below 1000 km, the negative ions play a dominant role. Besides, as the average charge number of the negative ions and dust grains is estimated to be >1 (Shebanits et al., 2016), the negative charge born by the negative ions could be higher compared to electrons for a same density. In the repartition of the electrons, a strong difference appears between the dayside and the nightside. P_2 electrons dominate the nightside whereas P_3 electrons play the main role on dayside.

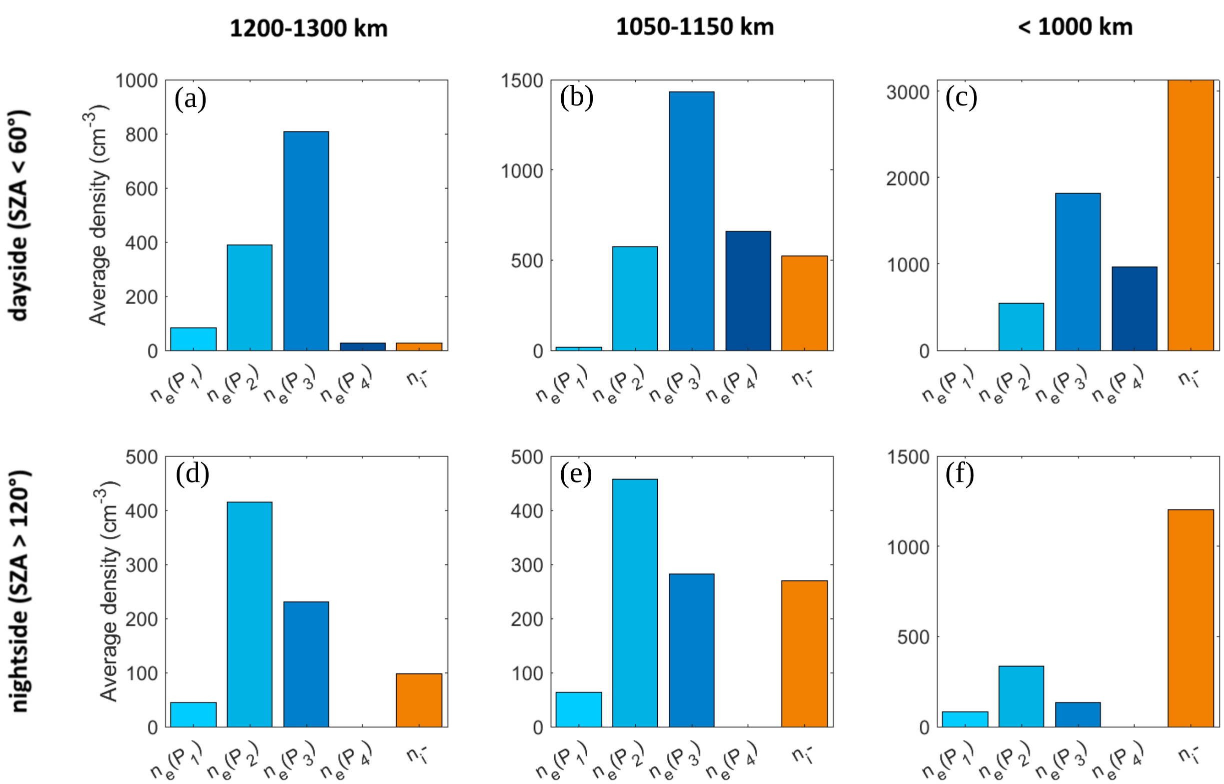

Figure 4. Average densities of negative charge carriers (the four electron populations and the negative ions). Comparison at different altitudes, (a,b,c) on dayside (SZA < 60°) and (d,e,f) on nightside (SZA > 120°).

3.3 Variations of the electron temperature with SZA and altitude

Figure 5 shows the variation of electron temperature with SZA for each of the four populations. At higher altitudes, above 1250 km, no strong differences are observed with SZA. However, with decreasing altitudes from 1250 to 850 km, a differentiation occurs between dayside and nightside measurements.

Concerning population P_1 (Figure 5a), there is a neat separation between two blocks below 1050 and 1250 km, that we name C1 and C2. C1 corresponds to cold electrons (< 0.03 eV, 350 K) present on nightside, down to the lower altitudes reached by the spacecraft. On the dayside, C2 hotter electrons (0.07-0.12 eV, 810-1390 K) are observed, but only above 1050 km. However, this can be due to the fact that the currents from P_2 and P_3 increase strongly and possibly cover the P_1 current (see paper I).

As is evident from Figure 2, the electrons of populations P_2 (Figure 5b) and P_3 (Figure 5c) get colder with decreasing altitude. However, at a given altitude, the temperatures of P_2 and P_3 are globally constant with SZA. This was previously observed with the analyses of one single electron population (Ågren et al., 2009). Only a small difference is observed below 1050 km: electrons on nightside seems slightly hotter (+0.01-0.02 eV), for SZA > 130° in the case of P_2, and for SZA > 100° in the case of P_3. Nevertheless, these values are within the fit error bars.

In the case of P_4, Figure 5d shows a sharp limit at 90° SZA: no electrons from the P_4 family can be observed on the nightside. Therefore, P_4 electrons appear only in sunlit regions. However, there is no relation between the electron temperature and the SZA.

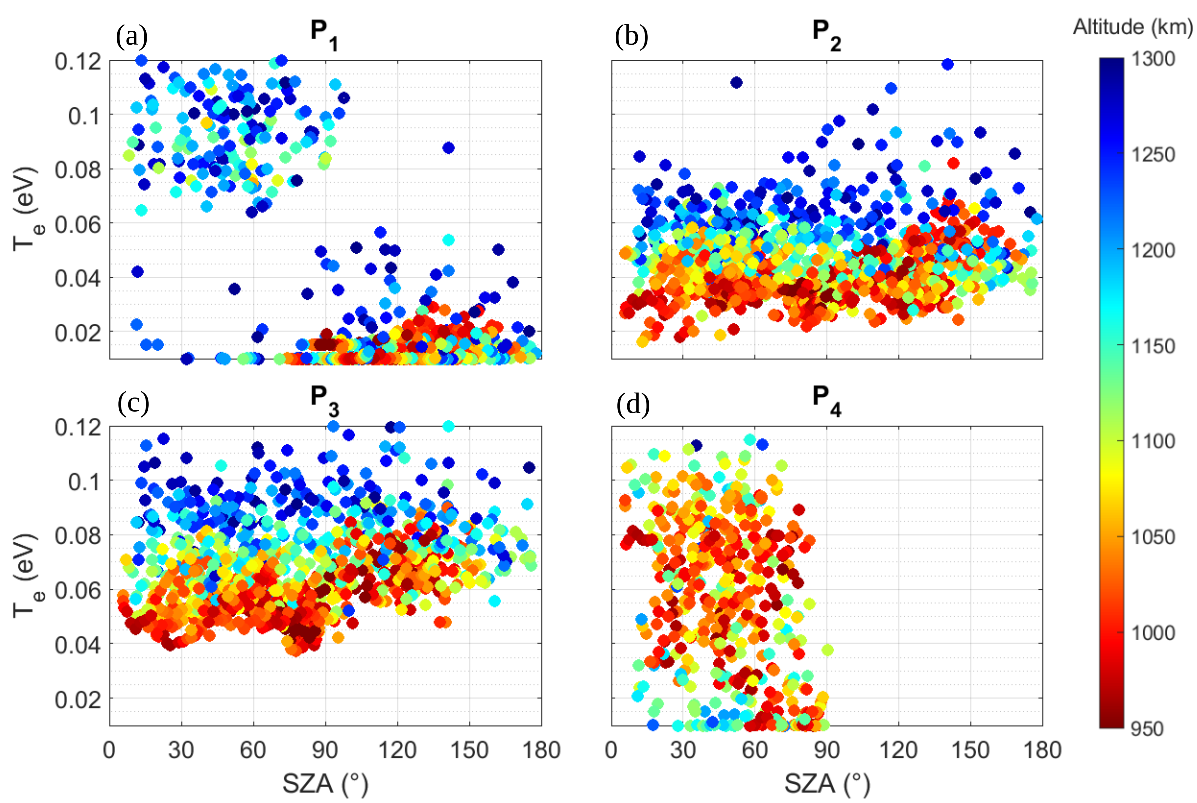

Figure 5. Electron temperature as a function of SZA and altitude for the four electron populations: (a) P_1, (b) P_2, (c) P_3 and (d) P_4. Data from 57 flybys.

3.4 Relation between the P_4 electron density and temperature

At a given altitude, electrons from P_2 and P_3 do not show any variation in temperature with density. For those populations, the temperature seems essentially governed by altitude. However, results are very different for population P_4. Figure 6 shows a linear trend between electron temperature and density, observed at all altitudes where P_4 electrons are detected. The linear coefficient varies with altitude from +0.016 eV (190 K) / 100 cm^{-3} at 1150-1250 km (Figure 6a) to +0.006 eV (80 K) / 100 cm^{-3} below 1050 km (Figure 6c) for SZA < 70°. Below 1050 km (Figure 6c), the slope varies also with SZA, and near the terminator (SZA > 70°) the coefficient is higher (+0.011 eV (130 K) / 100 cm^{-3}).

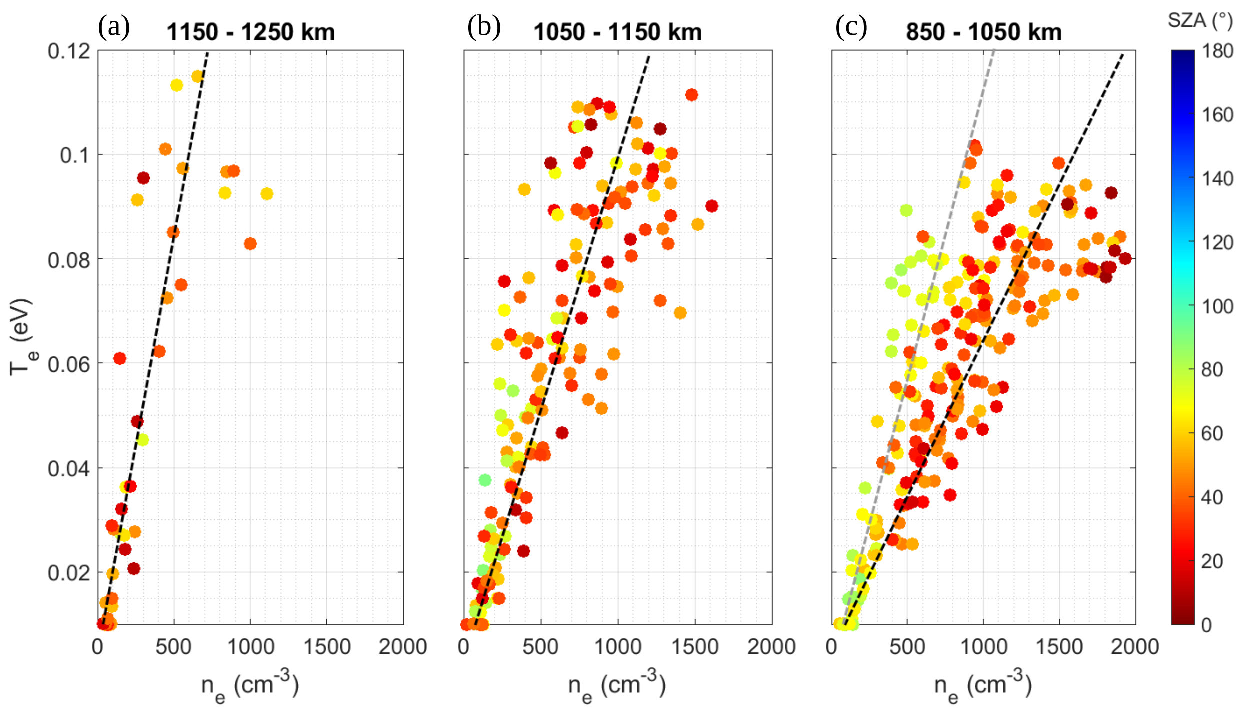

Figure 6. Electron temperature as a function of density and Solar Zenith Angle (SZA) in the case of population P4 at 3 different altitudes: (a) 1150-1250 km, (b) 1050-1150 km and (c) 850-1050 km. Data from 34 flybys on dayside. Linear trends are indicated with a black dashed line for SZA < 70° [(a) +0.016 eV/100 cm^{-3}, (b) +0.010 eV/100 cm^{-3} and (c) +0.006 eV/100 cm^{-3}], and with a grey dashed line for SZA > 70° below 1050 km [(c) +0.011 eV/100 cm^{-3}].

4 Correlations with UV fluxes, seasons and ion densities

4.1 Correlations with extreme UV fluxes

Extreme ultraviolet (EUV) fluxes used in this work are computed by Shebanits et al. (2017b) at the distance of Saturn from the solar irradiance measurements by the Solar EUV Experiment (SEE) instrument from the Thermosphere Ionosphere Mesosphere Energetics and Dynamics (TIMED) mission and the Solar Stellar Irradiance Comparison Experiment (SOLSTICE) from the Solar

Radiation and Climate Experiment (SORCE) mission (https://lasp.colorado.edu/lisird/). Therefore, EUV measurements in this study refer to the unattenuated solar EUV flux at the top of Titan's ionosphere.

Correlations observed with EUV fluxes depends on the population chosen. P_1 and P_2 are globally not EUV dependent. Only the P_1 electron temperature on dayside slightly increases with the EUV flux (+0.01 eV (115 K) every 0.1×10^{-4} W.m^{-2}), as shown on Figure 7a.

Nevertheless, a varying EUV flux as an effect on P_3 (plotted below 1000 km on Figure 7b) and P_4 (Figure 7c) densities. Below 1000 km, P_3 density increases roughly linearly, of +300 cm^{-3} every 0.1×10^{-4} W.m^{-2}. In parallel, P_4 denser cases are only observed at higher EUV fluxes.

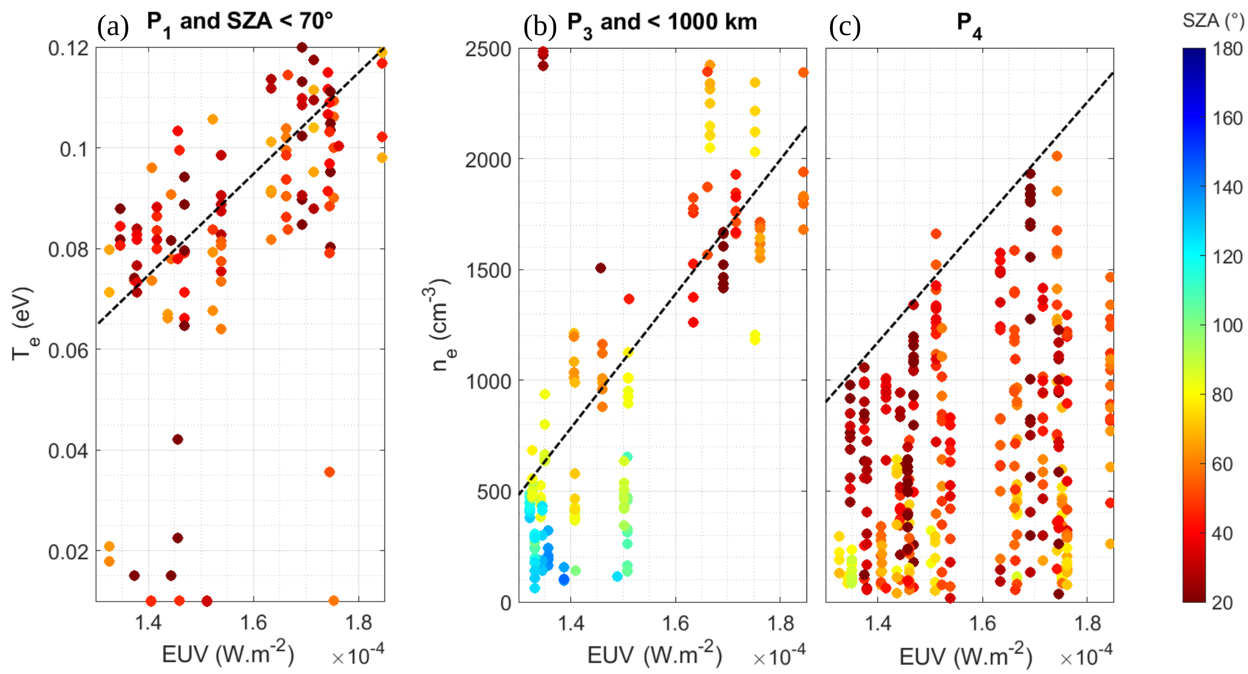

Figure 7. Electron characteristics as a function of extreme UV flux (integrated between 0.5-160.5 nm). (a) P_1 electron temperature for SZA < 70°. (b) P_3 electron density below 1000 km. (c) P_4 electron density. Linear trends are indicated with a black dashed line: (a) +0.01 eV/0.1×10^{-4} W.m^{-2}, (b) +300 cm^{-3}/0.1×10^{-4} W.m^{-2} and (c) +275 cm^{-3}/0.1×10^{-4} W.m^{-2}.

4.2 Impact of seasons and solar cycles

The Cassini mission covered two seasons in the Saturnian system, from the beginning of winter in the northern hemisphere to the summer solstice (May 2017). The Langmuir probe took measurements all over the mission, which enables to study the evolution of electron density and temperature with seasons (Edberg et al., 2013; Shebanits et al., 2017b).

The previous sections show that SZA affect electron populations, changing their densities and temperatures. Therefore, it is necessary to compare results at different seasons obtained with similar SZA. Figure 8a presents SZA during flybys as a function of seasons (latitude and date). In the case of SZA > 70°, two blocks of data have sufficient data points to be compared: one from

2006 to 2008 in the southern hemisphere (further named 'B1') and one from 2012 to 2014 in the northern hemisphere ('B2').

Figure 8b shows the evolution of the P_1 electron temperature for SZA < 70°. A higher temperature is observed in the 'B2' part than in the 'B1' part. Neither P_2 density nor temperature at a given altitude shows variations with latitude and seasons. Concerning P_3 electrons, their temperature is not affected by seasons and latitude, but their density in the cases where SZA < 70° is globally higher in the 'B2' part than in 'B1'. Figure 8d illustrates this effect with data points acquired below 1100 km. As for the population P_4, a similar effect is seen on both the electron density (Figure 8f) and temperature, as a linear correlation links its density and temperature (see Section 3.4).

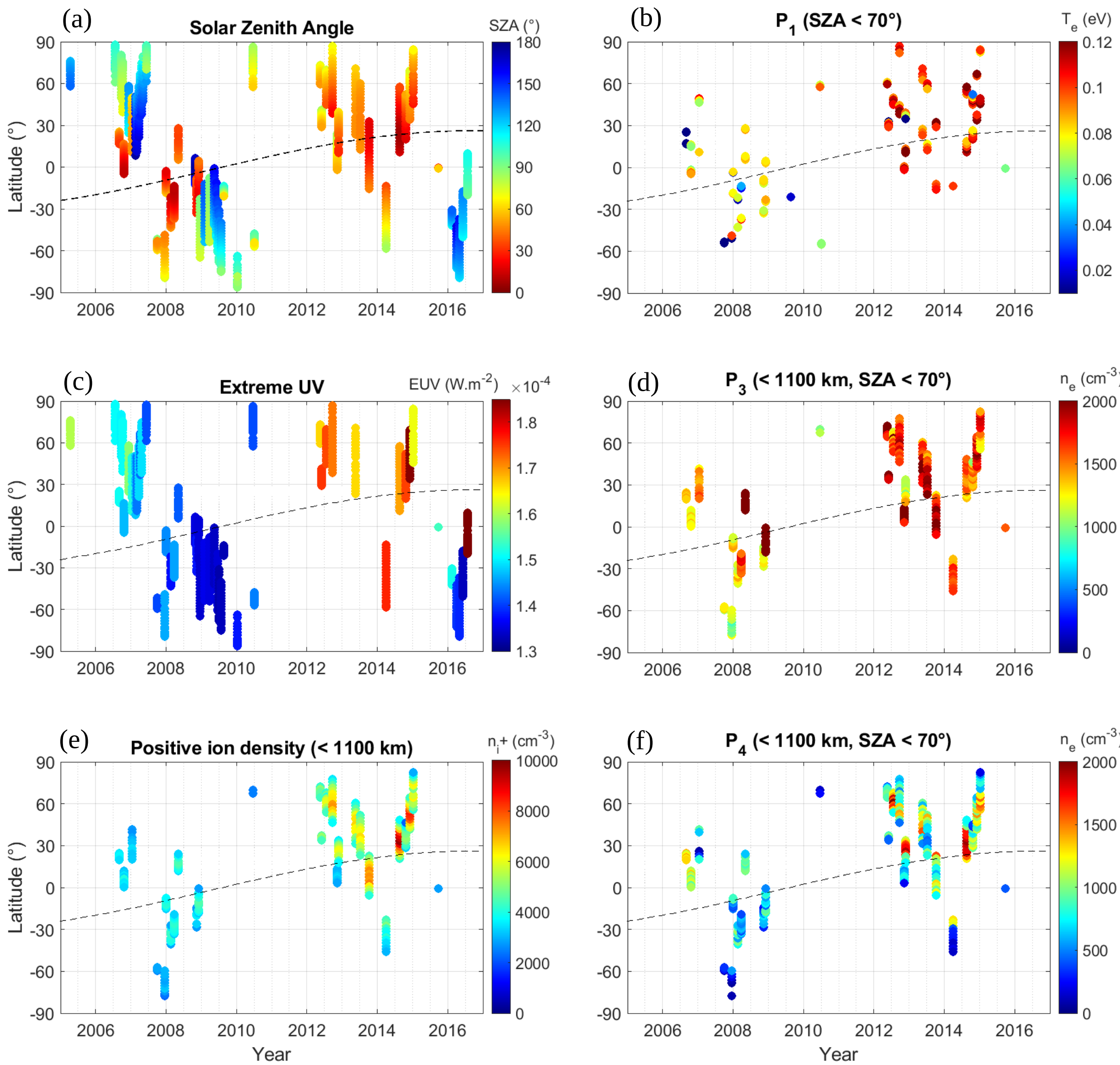

Figure 8. Evolution with seasons: (a) solar zenith angle during the flybys, (b) P_1 electron temperature on dayside, (d,f) P_3 and P_4 electron densities on dayside below 1100 km, (c) extreme UV flux (integrated between 0.5-160.5 nm) and (e) positive ion density below 1100 km (data from Shebanits et al., 2017b). The sub-solar latitude is indicated in black dashed line.

In conclusion, on dayside, P_3 and P_4 electrons are denser in the northern hemisphere from 2012 to 2014 (northern spring) than in the southern hemisphere from 2006 to 2008 (southern summer). Similarly, P_1 and P_4 electrons are hotter during the northern spring than during the southern summer. These observations are anti-correlated with the evolution of the Saturn-Sun distance, which was at its closest in 2003 (9 A.U.) and at its furthest in 2018 (10 A.U.).

Figure 8c presents the extreme UV flux and shows a good correlation with Figure 8b and 8d. The observed effect is then certainly linked to the variations of the EUV flux with years. In addition, these observations are correlated with the solar cycle that was at a minimum between 2005 and 2011 and at a maximum between 2011 and 2016. In conclusion, the modifications of the P_1 and P_4 electron temperatures and P_3 and P_4 densities in long time scales is mainly due to the evolution of EUV flux along the solar cycle, which has a greatest influence than seasons. This effect of the solar cycle on the total electron density has already been observed in 2013 (Edberg et al., 2013).

Finally, Figure 8e shows the evolution of positive ion density measured by Shebanits et al. (2017b) plotted similar to the graphs for P_3 and P_4 electrons in Figure 8d and 8f for easy comparison. We note similarities with P_3 and P_4, suggesting a correlation between these electron populations, the ion density and the EUV flux. Besides, a strong dependence between ion densities and the EUV flux (and then the solar cycle) has been observed by Shebanits et al. (2017b).

4.3 Correlations with ion density

The positive and negative ion densities have previously been retrieved by Shebanits et al. (2016, 2017b), from the comparative study of different instruments on-board Cassini: the RWPS/LP, the Ion and Neutral Mass Spectrometer INMS, the Cassini Plasma Science Electron Spectrometer CAPS/ELS and Ions Beam Spectrometer CAPS/IBS. We use these results in the current section.

P_1 and P_2 electron densities do not show any correlation with the positive (n_i+) and negative (n_i-) ion densities, contrary to P_3 and P_4. Figure 9 plots the P_3 and P_4 electron densities as a function of the positive ion density. The altitude (a,b) and the SZA (c,d) are indicated to help the interpretation. The two last subfigures (e,f) show the negative ion density.

Three different domains can globally be distinguished depending on the positive ion density.

(1) For $n_i+ < 2300$ cm^{-3} (usually at high altitudes or on nightside), P_3 electron density is linearly correlated to the positive ion density with a linear coefficient $n_i+/n_e(P_3)$ close to 2: there are two positive ions for one P_3 electron. In these cases, there are no P_4 electrons.

(2) For a positive ion density between ~2300 and ~3500 cm^{-3}, the P_3 electron density reaches a plateau. The P_4 electrons appear and are linearly correlated to the positive ion density with a linear coefficient $n_i+/n_e(P_4)$ close to 2.

(3) For $n_i+ > 3500$ cm^{-3}, both P_3 and P_4 electron densities are constant with an increasing positive ion density. In these conditions, the positive ion charge density is no longer compensated by the electrons (P_1 and P_2 having low densities), but by negative ions that increase strongly. We observe that these cases deviating from the linear trend are all at the lowest altitudes and at higher ion and dust densities.

An exception to these 3 domains is observed in a few flybys at lower altitudes (< 975 km) on nightside, where P_3 electrons are at low density (< 500 cm^{-3}), P_4 electrons are absent, but still positive and negative ions are present in relatively high quantities.

Concerning electron temperatures, we observed no dependence with the ion densities. For P_2 and P_3, the temperature depends only on the altitude, and for P_4 the temperature depends on the P_4 density.

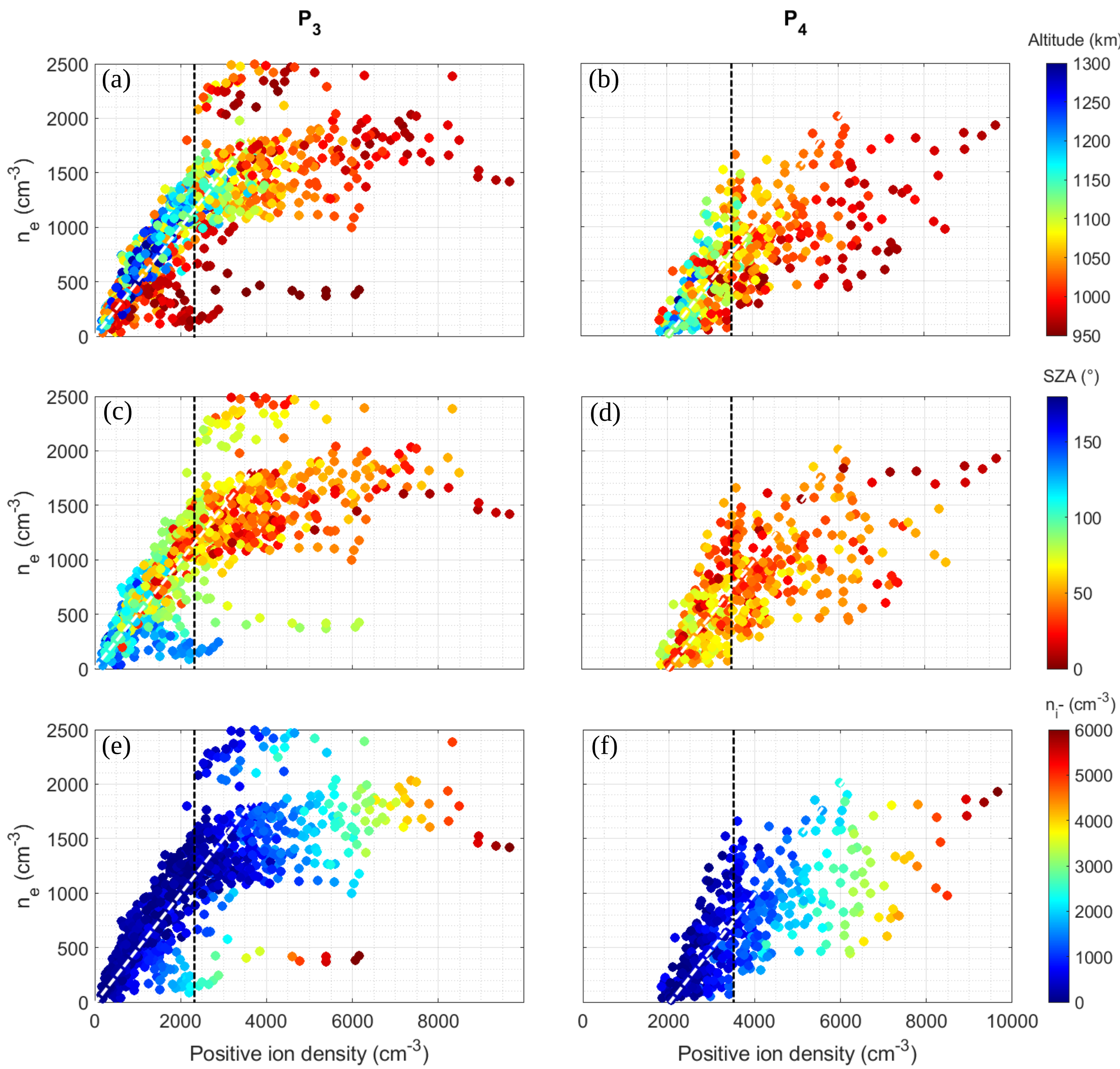

Figure 9. Correlation between P_3 (a,c,e) and P_4 (b,d,f) electron densities as a function of positive ion density. Colors refer to (a,b) altitude, (c,d) Solar Zenith Angle and (e,f) negative ion density. Positive and negative ion densities are from Shebanits et al. (2016, 2017b). Initial linear trends are indicated in white dotted lines ($n_i+/n_e = 2$). Trend transition zones are plotted in black dotted lines (2300 cm^{-3} for P_3, 3500 cm^{-3} for P_4)

5 Origins of the electron populations

5.1 Summary of the characteristics of the 4 populations

Table 1 summarizes the correlations observed in the previous sections between n_e, T_e, altitude, solar irradiation and ion density, for the 4 populations. Its content is described in Section 5.2, where it helps to suggest origins for the 4 populations.

Table 1. Summary of the correlations between n_e, T_e, altitude, solar irradiation and ion density, for the 4 populations.

Popula-tion	n_e, T_e	altitude	SZA, EUV, seasons	ions	suggested origin
P_1	**-n_e: constant and low** (~80 cm^{-3}) **-T_e: 2 cases**:, C1 < 0.02 eV, C2 ~0.1 eV	-C1: at all altitudes -C2: only above 1100 km	-C1 on nightside -C2 always present (and only) on dayside, T_e hotter at higher EUV fluxes.	/	electrons emitted from the probe by photons (C2) or energetic particles (C1)
P_2	/	**-n_e: globally constant** (500 cm^{-3}), slight shift at lower altitudes depending on SZA (400-700 cm^{-3}) **-T_e: linear decrease with decreasing altitude** (-0.01 eV / -100 km)	-n_e: at low altitude, slightly denser on dayside (x2).	/	thermaliza-tion of the suprathermal electrons coming from the magneto-sphere
P_3	/	**-n_e**: constant on nightside. **Linear increase on dayside with decreasing altitude** (+350 cm^{-3} / -100 km) **-T_e: linear decrease with decreasing altitude** (-0.017 eV / -100 km)	**-n_e: denser on dayside** (x6+) -below 1000 km, denser at higher EUV fluxes.	**-n_e: linear increase**, n_i+/n_e = 2 for n_i+ < 2300 cm^{-3}, constant above.	from photo-ionization of N_2 and CH_4, and ion chemistry
P_4	**-n_e and T_e proportional** (~0.01 eV / 100 cm^{-3})	**-only below 1200-1150 km** -denser cases are at lower altitudes	**- always present (and only) on dayside** -denser cases only at high EUV fluxes	**-n_e: linear increase**, n_i+/n_e = 2 for n_i+ < 4000 cm^{-3}, constant above.	from interaction of solar photons with aerosols or heavy negative ions

5.2 Suggested origins for the four populations

We discuss here possible origins for the four populations. They are schematized in Figure 10.

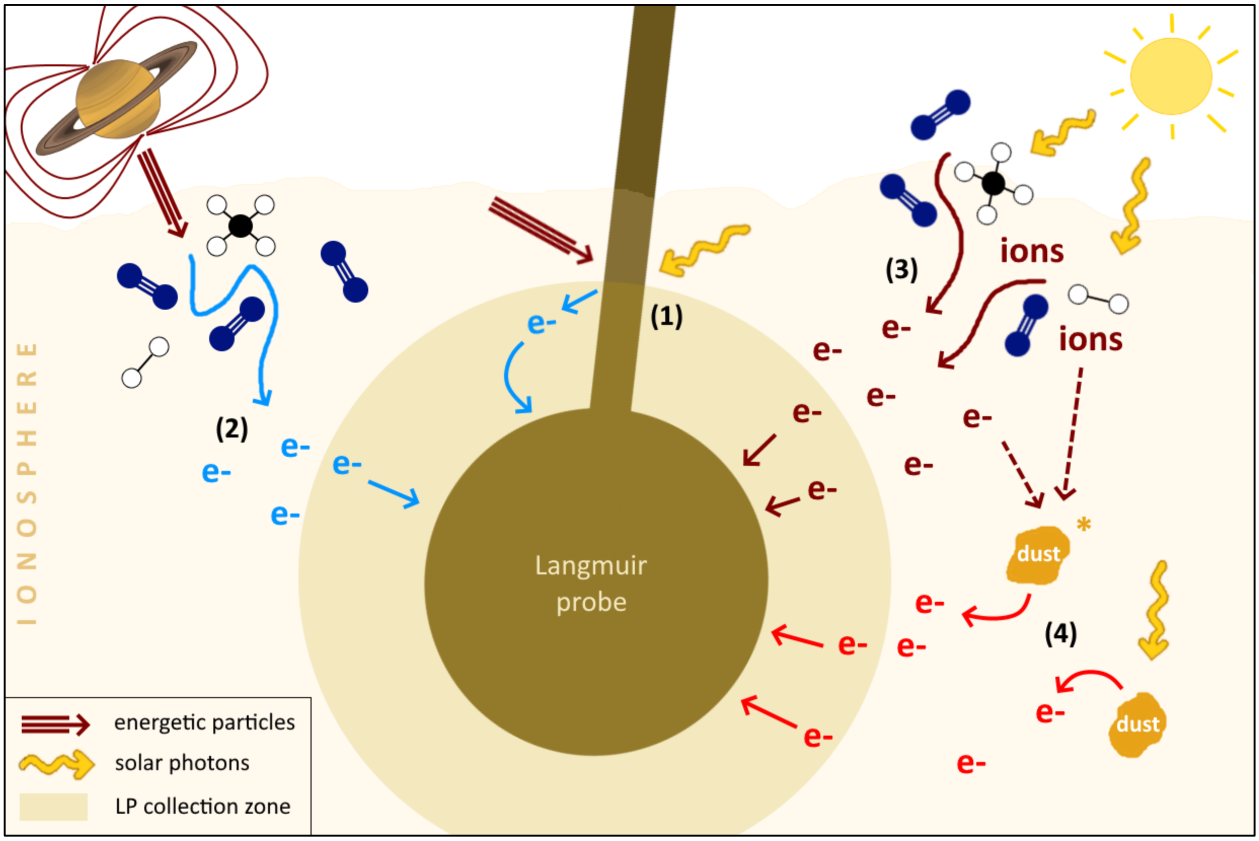

Figure 10. Scheme representing suggested origins for the 4 electron populations detected by the Langmuir probe in Titan's ionosphere. * next to a dust grain stands for 'excited'.

P_1 electrons are nearly always present and have a very low density. Their floating potential being the smallest of all the populations (see paper I), it is a strong indication that they are formed on the probe boom, emitted after collision with energetic photons or particles. Their higher temperature on dayside suggests that photo-emission forms more energetic electrons at the surface of the boom than secondary electrons emitted after collision with an energetic particle. On nightside, P_1 electron temperature is close to the 0.015 eV instrumental limitation, which could also affect the detection of this population.

The P_2 electron population depends only slightly on solar illumination. It has a constant density (~500 cm^{-3}) at all altitudes and solar zenith angles. It is always present, and is the major ion population on nightside. Its temperature decreases linearly with decreasing altitude, down to ~0.04 eV (460 K) at 1000 km. For these reasons, it is likely that P_2 electrons are background thermalized electrons, present in all the ionosphere of Titan. Their constancy with solar illumination indicates that they could mainly be due to the thermalization of suprathermal magnetospheric electrons.

P_3 and P_4 populations show strong correlations with the SZA and the EUV flux. Consequently, their origin must be linked to the solar irradiation. In addition, both have a density increasing with decreasing altitude. To summarize, increases in solar photons and atmospheric pressure (i.e. neutral density) lead to an enhanced formation of P_3 and P_4 electrons: these electrons are formed from the energy deposit of solar photons in the atmosphere. The main difference between the two populations is their temperature. P_3 electron temperature depends essentially on the altitude: a higher collision rate at higher pressure lead to a lower temperature. In contrast, the temperature of P_4 electrons depends mainly on their density: their temperature is higher when their density is higher. These points suggest a different origin for the two populations. P_3 electrons nearly appear at all altitudes, whereas P_4 electrons are confined below 1150-1200 km, where negative ions and dust particles are dominant. At the light of these observations, we suggest that P_3 electrons come from the photo-ionization of neutral atmospheric molecules (mainly CH_4 and N_2) and the subsequent ion chemistry, while P_4 electrons are formed on the dust grains or heavy negative ions by interaction with the solar photons.

5.3 Discussion on the dust origin of P_4

P_4 electrons are a clue of the interaction of the plasma with the aerosols in the ionosphere of Titan. Extracted from the aerosols, their floating potential is different from the plasma potential. This explains why the P_4 electrons are collected at a very different voltage bias of the probe than the other populations (see paper I).

A few hypotheses can be made on the processes forming electrons from the interaction of aerosols grains with solar photons. Photo-extraction from the bulk of the material requires strong UV photons (> 6 eV), while photo-desorption can happen with low energy photons (1-2 eV), but with lower efficiency. In these cases, the energy of the electron formed depends on the energy of the incident photon. This can explain the linear dependence between n_e and T_e: higher and stronger solar radiations lead to a higher quantity of P_4 electrons, and at higher energies. Tigrine et al. (2018) studied photo-emission of electrons on analogues of Titan's aerosols under VUV irradiation. Using an extrapolation of their data points, we observe that the formation of electrons at 0.1 eV would be possible and require incoming photons of ~6 eV.

Woodard et al. (2020) studied a laboratory dusty plasma with a Langmuir probe and also observed an unexpected electron population at a potential different from the plasma potential. They showed that the potential of the unexpected population is the same as the potential of the aerosols. Using numerical modeling they investigated its origin. In their conditions, the electron photo-emission and the secondary electron emission from the flux of charged species to the particle surface are not sufficient to explain the density of the new population. They propose another process: the thermo-emission of electrons from the nanoparticles, enhanced by electrostatic effects. Indeed, the aerosols are heated by the ion bombardment, the collection of electrons and the recombination of radicals and ions at their surface. The accumulated heat cannot be transferred to the background gas because of the low pressure and the inefficient radiation of small particles. On the other hand, the charge of the aerosols decreases the barrier for electron emission. In conclusion, the P_4 population observed on Titan could similarly be due to electron emission from the aerosols heated by the ion chemistry and the collection of the numerous electrons present on the dayside. In particular, a previous experimental work done by Chatain et al. (2020) showed that analogues to Titan's aerosols are chemically modified by exposure to a laboratory plasma mimicking Titan's ionosphere, which could participate to the heating of the aerosols.

5 Conclusions

The re-analysis of the Cassini Langmuir probe dataset in the ionosphere of Titan below 1200 km led to a better understanding of this ionized environment. Paper I, which details the re-analysis method, discuss the presence of several electron populations that are not expected by the ionospheric models that predict only one thermalized electron population. Between 2 and 4 electron populations are detected depending on the solar illumination and altitude. In this second paper we analyzed the complete Langmuir probe dataset below 1200 km with the objective to characterize the four populations and find correlations through statistics.

A first population at very low density is attributed to photoelectrons or secondary electrons emitted by the probe boom. The second population is detected in all conditions, with a density ~500 cm^{-3} and temperature of 0.04 ± 0.02 eV (460 ± 230 K) at 1000 km altitude. It is attributed to background thermalized electrons, possibly originally coming from suprathermal magnetospheric electrons.

The two remaining populations are very sensitive to solar zenith angle and extreme UV fluxes. Their density also increases with pressure, suggesting that their formation processes deal with the deposition of solar photon energy into the ionosphere. They are the dominant electron populations on dayside. The third population is observed at all altitudes, on dayside (up to 2700 cm^{-3}) and in lower density on nightside near the terminator. Its temperature decreases with altitude, down to 0.06 eV ± 0.02 eV (700 ± 230 K) at 1000 km. It is suspected to be closely linked to the photo-ionization of the gas phase on dayside and to the subsequent ion chemistry induced. On the opposite, the fourth population is rigorously observed only on dayside and below 1200 km altitude, and its temperature is linearly correlated to its density (up to 0.12 eV / 1390 K and 2000 cm^{-3}). Its origin could be related to the presence of dust exposed to solar photons and active ion chemistry, through photo- or thermo-emission.

Acknowledgments and Data

The Swedish National Space Board (SNSB) supports the RPWS/LP instrument on board Cassini. A.C. acknowledges ENS Paris-Saclay Doctoral Program. O.S. acknowledges funding by the Royal Society grant RP\EA\180014. N.J.T.E. was funded by the Swedish National Space Board under contract 135/13 and by the Swedish Research Council under contract 621-2013-4191. N.C. acknowledges the financial support of the European Research Council (ERC Starting Grant PRIMCHEM, Grant agreement no. 636829).

All Cassini RPWS data are archived in the Planetary Data System (PDS) Planetary Plasma Interaction (PPI) node at https://pds-ppi.igpp.ucla.edu on a pre-arranged schedule. The authors thank the TIMED/SEE and SORCE/SOLSTICE instruments' teams for providing the solar irradiance data, available at http://lasp.colorado.edu/lisird/data/timed_see_ssi_l3/ and http://lasp.colorado.edu/lisird/data/sorce_ssi_l3/, respectively.

References

Ågren, K., Wahlund, J.-E., Garnier, P., Modolo, R., Cui, J., Galand, M., & Müller-Wodarg, I. (2009). On the ionospheric structure of Titan. *Planetary and Space Science*, *57*(14–15), 1821–1827. https://doi.org/10.1016/J.PSS.2009.04.012

Chatain, A., Wahlund, J. -E., Shebanits, O., Hadid, L. Z., Eriksson, A. I., Morooka, M. W., et al. (n.d.). Re-analysis of the Cassini RPWS/LP data in Titan's ionosphere. Part I: detection of several electron populations. *Journal of Geophysical Research: Space Physics, submitted*.

Chatain, A., Carrasco, N., Ruscassier, N., Gautier, T., Vettier, L., & Guaitella, O. (2020). Interaction dust – plasma in Titan's ionosphere: an experimental simulation of aerosols erosion. *Icarus*, *345*, 113741. https://doi.org/10.1016/j.icarus.2020.113741

Coates, A. J., Crary, F. J., Lewis, G. R., Young, D. T., Waite, J. J. H., & Sittler, J. E. C. (2007). Discovery of heavy negative ions in Titan's ionosphere. *Geophysical Research Letters*, *34*, L22103. https://doi.org/10.1029/2007GL030978

Coates, A. J., Wellbrock, A., Lewis, G. R., Jones, G. H., Young, D. T., Crary, F. J., & Waite, J. H. (2009). Heavy negative ions in Titan's ionosphere: Altitude and latitude dependence. *Planetary and Space Science*, *57*(14–15), 1866–1871. https://doi.org/10.1016/j.pss.2009.05.009

Crary, F. J., Magee, B. A., Mandt, K., Waite, J. H., Westlake, J., & Young, D. T. (2009). Heavy ions, temperatures and winds in Titan's ionosphere: Combined Cassini CAPS and INMS observations. *Planetary and Space Science*, *57*(14–15), 1847–1856. https://doi.org/10.1016/j.pss.2009.09.006

Cui, J., Yelle, R. V., Vuitton, V., Waite, J. H., Kasprzak, W. T., Gell, D. A., et al. (2009). Analysis of Titan's neutral upper atmosphere from Cassini Ion Neutral Mass Spectrometer measurements. *Icarus*, *200*(2), 581–615. https://doi.org/10.1016/j.icarus.2008.12.005

Edberg, N. J. T., Wahlund, J. E., Ågren, K., Morooka, M. W., Modolo, R., Bertucci, C., & Dougherty, M. K. (2010). Electron density and temperature measurements in the cold plasma environment of Titan: Implications for atmospheric escape. *Geophysical Research Letters*, *37*, L20105. https://doi.org/10.1029/2010GL044544

Edberg, N. J. T., Andrews, D. J., Shebanits, O., Ågren, K., Wahlund, J. E., Opgenoorth, H. J., et al. (2013). Solar cycle modulation of Titan's ionosphere. *Journal of Geophysical Research: Space Physics*, *118*(8), 5255–5264. https://doi.org/10.1002/jgra.50463

Edberg, N. J. T., Andrews, D. J., Bertucci, C., Gurnett, D. A., Holmberg, M. K. G., Jackman, C. M., et al. (2015). Effects of Saturn's magnetospheric dynamics on Titan's ionosphere. *Journal of Geophysical Research: Space Physics*, *120*(10), 8884–8898. https://doi.org/10.1002/2015JA021373

Eriksson, A. I., Engelhardt, I. A. D., André, M., Boström, R., Edberg, N. J. T., Johansson, F. L., et al. (2017). Cold and warm electrons at comet 67P/Churyumov-Gerasimenko. *Astronomy and Astrophysics*, *605*. https://doi.org/10.1051/0004-6361/201630159

Galand, M., Coates, A. J., Cravens, T. E., & Wahlund, J.-E. (2014). Titan's Ionosphere. In *Titan* (pp. 296–361). Cambridge, UK: Cambridge University Press.

Gurnett, D. A., Kurth, W. S., & Scarf, F. L. (1981). Plasma waves near Saturn: Initial results from Voyager 1. *Science*, *212*(4491), 235–239. https://doi.org/10.1126/science.212.4491.235

Gurnett, D. A., Kurth, W. S., Kirchner, D. L., Hospodarsky, G. B., Averkamp, T. F., Zarka, P., et al. (2004). The Cassini Radio and Plasma Wave Investigation. In *The Cassini-Huygens Mission* (pp. 395–463). Springer Netherlands. https://doi.org/10.1007/978-1-4020-2774-1_6

Hanson, W. B., & Mantas, G. P. (1988). Viking electron temperature measurements: Evidence for a magnetic field in the Martian ionosphere. *Journal of Geophysical Research*, *93*(A7), 7538. https://doi.org/10.1029/ja093ia07p07538

Intriligator, D. S., Collard, H. R., Mihalov, J. D., Written, R. C., & Wolfe, J. H. (1979). Electron observations and ion flows from the Pioneer Venus orbiter plasma analyzer experiment. *Science*, *205*(4401), 116–119. https://doi.org/10.1126/science.205.4401.116

Magee, B. A., Waite, J. H., Mandt, K. E., Westlake, J., Bell, J., & Gell, D. A. (2009). INMS-derived composition of Titan's upper atmosphere: Analysis methods and model comparison. *Planetary and Space Science*, *57*(14–15), 1895–1916. https://doi.org/10.1016/j.pss.2009.06.016

Mandt, K. E., Gell, D. A., Perry, M., Hunter Waite, J., Crary, F. A., Young, D., et al. (2012). Ion densities and composition of Titan's upper atmosphere derived from the Cassini Ion Neutral Mass Spectrometer: Analysis methods and comparison of measured ion densities to photochemical model simulations. *Journal of Geophysical Research E: Planets*, *117*(10). https://doi.org/10.1029/2012JE004139

Mitchell, D. L., Lin, R. P., Rème, H., Crider, D. H., Cloutier, P. A., Connerney, J. E. P., et al. (2000). Oxygen Auger electrons observed in Mars' ionosphere. *Geophysical Research Letters*, *27*(13), 1871–1874. https://doi.org/10.1029/1999GL010754

Mukundan, V., & Bhardwaj, A. (2018). Dayside ionosphere of Titan: Impact on calculated plasma densities due to variations in the model parameters. *Icarus*, *299*, 222–239. https://doi.org/10.1016/j.icarus.2017.07.022

Richard, M. S., Cravens, T. E., Robertson, I. P., Waite, J. H., Wahlund, J.-E., Crary, F. J., & Coates, A. J. (2011). Energetics of Titan's ionosphere: Model comparisons with Cassini data. *Journal of Geophysical Research: Space Physics*, *116*, A09310. https://doi.org/10.1029/2011JA016603

Scarf, F. L., Gurnett, D. A., Kurth, W. S., & Poynter, R. L. (1982). Voyager 2 plasma wave observations at Saturn. *Science*, *215*(4532), 587–594. https://doi.org/10.1126/science.215.4532.587

Schippers, P., Blanc, M., André, N., Dandouras, I., Lewis, G. R., Gilbert, L. K., et al. (2008). Multi-instrument analysis of electron populations in Saturn's magnetosphere. *Journal of Geophysical Research: Space Physics*, *113*(7), 1–10. https://doi.org/10.1029/2008JA013098

Shebanits, O., Wahlund, J.-E., Edberg, N. J. T., Crary, F. J., Wellbrock, A., Andrews, D. J., et al. (2016). Ion and aerosol precursor densities in Titan's ionosphere: A multi-instrument case study. *Journal of Geophysical Research: Space Physics*, *121*(10), 10,075-10,090. https://doi.org/10.1002/2016JA022980

Shebanits, O., Vigren, E., Wahlund, J.-E., Edberg, N. J. T., Cui, J., Mandt, K. E., & Waite, J. H.

(2017a). Photoionization Modeling of Titan's Dayside Ionosphere. *The Astrophysical Journal*, *850*(2), L26. https://doi.org/10.3847/2041-8213/aa998d

Shebanits, O., Vigren, E., Wahlund, J. E., Holmberg, M. K. G., Morooka, M., Edberg, N. J. T., et al. (2017b). Titan's ionosphere: A survey of solar EUV influences. *Journal of Geophysical Research: Space Physics*, *122*(7), 7491–7503. https://doi.org/10.1002/2017JA023987

Tigrine, S., Carrasco, N., Bozanic, D. K., Garcia, G. A., & Nahon, L. (2018). FUV Photoionization of Titan Atmospheric Aerosols. *The Astrophysical Journal*, *867*(2), 164. https://doi.org/10.3847/1538-4357/aae4d8

Tokar, R. L., Johnson, R. E., Hill, T. W., Pontius, D. H., Kurth, W. S., Crary, F. J., et al. (2006). The interaction of the atmosphere of Enceladus with Saturn's plasma. *Science, 311*(5766), 1409–1412. https://doi.org/10.1126/science.1121061

Veszelei, M. (1997). Preparation and characterization of sputtered metal oxides and nitrides for optical applications. *Doctoral Dissertation, Acta Universitatis Upsaliensis*.

Vigren, E., Galand, M., Yelle, R. V., Cui, J., Wahlund, J. E., Ågren, K., et al. (2013). On the thermal electron balance in Titan's sunlit upper atmosphere. *Icarus*, *223*(1), 234–251. https://doi.org/10.1016/j.icarus.2012.12.010

Vigren, E., Galand, M., Wellbrock, A., Coates, A. J., Cui, J., Edberg, N. J. T., et al. (2016). Suprathermal electrons in Titan's sunlit ionosphere: model-observation comparisons. *The Astrophysical Journal*, *826*(2), 131. https://doi.org/10.3847/0004-637x/826/2/131

Vuitton, V., Yelle, R. V., Klippenstein, S. J., Hörst, S. M., & Lavvas, P. (2019). Simulating the density of organic species in the atmosphere of Titan with a coupled ion-neutral photochemical model. *Icarus*, *324*, 120–197. https://doi.org/10.1016/j.icarus.2018.06.013

Wahlund, J. E., Boström, R., Gustafsson, G., Gurnett, D. A., Kurth, W. S., Pedersen, A., et al. (2005). Cassini measurements of cold plasma in the ionosphere of Titan. *Science*, *308*(5724), 986–989. https://doi.org/10.1126/science.1109807

Waite, J. H., Niemann, H., Yelle, R. V., Kasprzak, W. T., Cravens, T. E., Luhmann, J. G., et al. (2005). Ion Neutral Mass Spectrometer results from the first flyby of Titan. *Science*, *308*(5724), 982–986. https://doi.org/10.1126/science.1110652

Waite, J. H., Young, D. T., Cravens, T. E., Coates, A. J., Crary, F. J., Magee, B., & Westlake, J. (2007). Planetary science: The process of tholin formation in Titan's upper atmosphere. *Science*, *316*(5826), 870–875. https://doi.org/10.1126/science.1139727

Wellbrock, A., Coates, A. J., Jones, G. H., Lewis, G. R., & Waite, J. H. (2013). Cassini CAPS-ELS observations of negative ions in Titan's ionosphere: Trends of density with altitude. *Geophysical Research Letters*, *40*(17), 4481–4485. https://doi.org/10.1002/grl.50751

Wellbrock, A., Coates, A. J., Jones, G. H., Vuitton, V., Lavvas, P., Desai, R. T., & Waite, J. H. (2019). Heavy negative ion growth in Titan's polar winter. *Monthly Notices of the Royal Astronomical Society*, *490*(2), 2254–2261. https://doi.org/10.1093/mnras/stz2655

Woodard, A., Shojaei, K., Berrospe-Rodriguez, C., Nava, G., & Mangolini, L. (2020). Electron emission from particles strongly affects the electron energy distribution in dusty plasmas. *Journal of Vacuum Science & Technology A*, *38*, 023005. https://doi.org/10.1116/1.5134706